Characterisation and evaluation of paramagnetic fluorine labelled glycol chitosan conjugates for ^{19}F and ^{1}H magnetic resonance imaging

Elena De Luca, Peter Harvey, Kirsten H. Chalmers, Anurag Mishra, P. Kanthi Senanayake, J Ian Wilson, Mauro Botta, Marianna Fekete, Andrew M. Blamire, and David Parker

Received June 25 2013

E. De Luca, P. Harvey, K.H. Chalmers, A. Mishra, P. K. Senanayake, D. Parker
Department of Chemistry, Durham University, South Road, Durham DH1 3LE, United Kingdom.

J. I. Wilson, A. M. Blamire
Northern Institute for Cancer Research, and Institute of Cellular Medicine Newcastle University, Newcastle upon Tyne, NE4 5PL, United Kingdom.

M. Botta, M. Fekete
Dipartimento di Scienze e Innovazione Tecnologica, Università del Piemonte Orientale "Amedeo Avogadro", Viale Teresa Michel 11, 15121 Alessandria, Italy

Abstract Medium molecular weight conjugates of glycol-chitosan have been prepared, linked by an amide bond to paramagnetic Gd(III), Ho(III) and Dy(III) macrocyclic complexes in which a trifluoromethyl reporter group is located 6.5Å from the paramagnetic centre. The faster relaxation of the observed nucleus allows modified pulse sequences to be used with shorter acquisition times. The polydisperse materials have been characterized by gel permeation chromatography, revealing an average MW of the order of 13,800 (Gd), 14,600 (Dy) and 16,200 (Ho), consistent with the presence of 8.5, 9.5 and 13 complexes respectively. The Gd conjugate was prepared for both a q = 1 monoamide-tricarboxylate conjugate (r_{1p} 11.2 $mM^{-1}s^{-1}$, 310K, 1.4T) and a q = 0 triphosphinate system and conventional contrast enhanced proton MRI studies at 7T undertaken in mice bearing an HT-29 or an HCT-116 colorectal tumour xenograft (17μmol/kg). Enhanced contrast was observed following injection in the tail vein in tumour tissue, with uptake also evident in the liver and kidney with a tumour/liver ratio of 2:1 at 13 minutes, and large amounts in the kidney and bladder consistent with predominant renal clearance. Parallel experiments observing the ^{19}F resonance in the Ho conjugate complex using a surface coil did not succeed owing to its high R_2 value (750Hz, 7T). However, the fluorine signal in the Dy triphosphinate chitosan conjugate (R_1/R_2 = 0.6 and R_1 = 145 Hz (7T)) was sharper and could be observed *in vivo* at -65.7 ppm, following intravenous tail vein injection of a dose of 34 μmol/kg.

Keywords Contrast agents, fluorine, tumour uptake, MRI, imaging

Abbreviations

NMM	N-methyl morpholine
TBTU	Tetramethyluronium tetrafluoroborate
GPC	gel permeation chromatography
DO3A	1,4,7-tricarboxymethyl-1,4,7,10-tetraazacyclododecane
PDI	polydispersity index
MRI	magnetic resonance imaging
MRSI	magnetic resonance spectroscopic imaging

Introduction

Fluorine magnetic resonance imaging has been promoted as an alternative to proton MRI or MRSI, due to the 100% isotopic abundance of the ^{19}F nucleus, the high NMR sensitivity and near zero background signal. [1,2] Over the past 20 years, notwithstanding the use of dedicated imaging coils, such work has been limited to observation of probes with high spin-density, e.g. locally injected perfluoralkyl and perfluoro-crown ether suspensions. Overall, limited impact has occurred and only sporadic applications reported. [3] Over the past 5 years, we have shown that improvements in sensitivity of between 10 and 25-fold can be gained in ^{19}F MR imaging, by placing a reporter trifluoromethyl group between 4.5 and 7Å from a paramagnetic centre, such as a lanthanide ion (in particular: the faster relaxing and shifting ions: Dy, Tb Ho, Er and Tm). [4,5] Too close and line-broadening is very severe; too distant and the relaxation rate enhancement is very small. An alternative approach has been suggested using a proximate Fe^{3+} or Mn^{2+} centre, in the context of monitoring enzymatic transformations by ^{19}F NMR, although rate enhancements were rather lower than ideal in the cases cited. [6] For rates of longitudinal relaxation of between 50 and 250 Hz, much shorter acquisition times can be used, including the use of a 'zero-echo time' imaging pulse sequence. [7] These approaches are generally applicable to any spin ½ nucleus, and require that the R_1/R_2 ratio is as close as possible to unity and that R_2 is preferably no greater than 300 to 500 Hz. Otherwise, concomitant broadening of the signal inhibits observation in spectroscopy. In imaging, if R_2 becomes large, "T_2 losses" occur during acquisition, associated with the longer RF pulse required and the spatial encoding process, limiting any intrinsic sensitivity gains.

A further aspect of this approach to more practicable ^{19}F imaging is that the spin density should be maximised within the region of interest that is observed. The use of low MW fluorine labelled lanthanide complexes *per se* is constrained by their rapid rates of clearance, following intravenous introduction into the body. With this in mind, we have set out to study medium MW polydisperse conjugates, in which about 30 fluorine nuclei (i.e. 10 CF_3 groups, on average) are linked to a biocompatible vector. Such an approach has one main benefit in that the material will tend to clear more slowly from the body, as diffusion into the extravascular space is retarded. Such behaviour will increase the opportunities for ^{19}F imaging of probe location, prior to

excretion. The use of a conjugate that is readily metabolised by the action of natural glycosidase enzymes was also considered to offer advantages in ensuring longer term whole body clearance, as the lower molecular weight monomeric complexes are normally expected to clear rapidly via the renal or biliary routes.

In this work, monomeric CF_3 labelled lanthanide complexes have been used as they are kinetically inert with respect to premature dissociation of the metal ion in vivo. [8,9] Thus, complexes of monoamide-tricarboxylate and triphosphinate derivatives of 1,4,17,10-tetraazacyclododecane have been used, as they have been shown to be resistant to acid catalysed dissociation pathways. [10] Furthermore, the CF_3 group is engineered to be about 6 to 6.5Å from the paramagnetic centre. At this distance and at a field of 7 T, this makes the complexes of Tb, Dy and Ho rational choices for exploration, as they possess R_1 values in the range 50-150 Hz, under these conditions. [4c, 11]

Chitosan is a linear polysaccharide composed of randomly distributed β-(1-4)-linked D-glucosamine and *N*-acetyl-D-glucosamine moieties. Importantly, it is non-toxic, biodegradable and is tolerated well *in vivo*. [12] It is produced *via* the de-acetylation of chitin and is a cheap and readily available high molecular weight vector for bio-conjugation work. The aqueous solubility is enhanced in the simple derivative, glycol-chitosan; this is commercially available. The material is polydisperse and, in this work, it was hydrolysed by acid digestion for 24h. [12-14] Such treatment generates a precursor in which the amide bonds are cleaved and the polysaccharide partially hydrolysed, to yield a material with an average of 35 monosaccharide units, in which the primary amine groups are amenable for conjugation. Thus, the conjugates [**Ln.L^1-chitosan**] and [**Ln.L^3-chitosan**] were studied, with [**Ln.L^2**] prepared as a control (Scheme 1). The corresponding Gd complexes serve as proton MRI contrast agents, catalyzing the rate of relaxation of the bulk water signal which is in proximity. Hence, proton MRI studies were undertaken first to define the location of the conjugate, and ^{19}F imaging studies attempted thereafter, aided by knowledge of the tissue distribution of the conjugate.

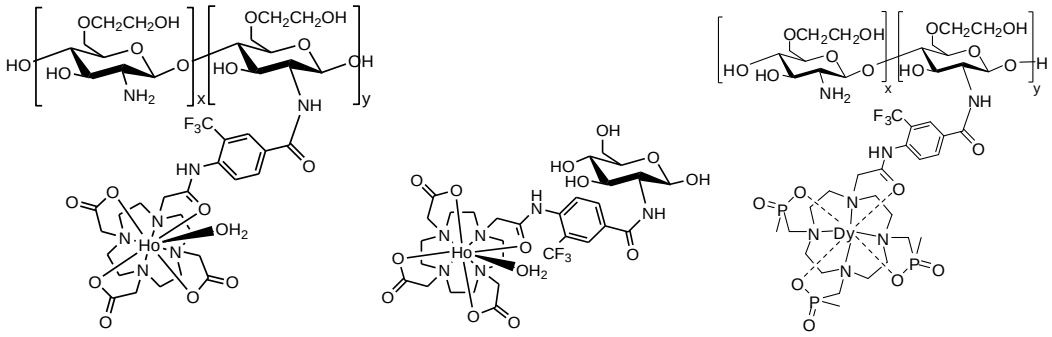

[Ho.L^1-chitosan(H$_2$O)] **[Ho.L^2(H$_2$O)]** **[Dy.L^3-chitosan]**

Scheme 1 Structures of complexes and conjugates studied

Materials and Methods

Gel Permeation Chromatography

Gel permeation chromatography (GPC) was undertaken at Smithers Rapra UK, using a Viscotek Model 301 TDA instrument with associated pump, autosampler, and refractive index detector (with differential pressure and light scattering). Agilent PLaquagel-OH Guard plus 2 x PLaquagel-OH Mixed-M, 30 cm, 8 μm columns were used with an eluent composed of 0.5 M $NaNO_3$, 0.01 M NaH_2PO_4 at pH 2 at a flow rate of 1.0 mL/min at 30°C. The GPC system was calibrated using Pullulan polysaccharides and the data analysed using Malvern/Viscotek 'OmniSec' software.

Mass Spectrometry

Both standard and high resolution electrospray mass spectrometry were recorded on a Thermo-Finnigan LTQ FT instrument, operating in positive or negative ion mode as stated, with MeOH as the carrier solvent. MALDI mass spectra were recorded on an Applied Biosystems Voyager-DE STR instrument with MeOH as the carrier solvent. LC-MS analyses were performed on a Waters system comprising a 3100 Mass Detector and a 2998 Photodiode array detector.

NMR Spectroscopy

^{1}H, ^{13}C, ^{19}F, and ^{31}P NMR spectra were recorded in commercially available deuterated solvents on a Varian Mecury-200 (^{1}H at 199.975 MHz, ^{13}C at 50.289 MHz, ^{19}F at 188.179 MHz, ^{31}P at 80.985 MHz), Varian Mercury-400 (^{1}H at 399.960 MHz, ^{13}C at 100.572 MHz, ^{19}F at 376.338 MHz, ^{31}P at 161.943 MHz), Bruker Avance-400 (^{1}H at 400.052 MHz, ^{13}C at 100.603 MHz, ^{19}F at 376.423 MHz, ^{31}P at 161.980 MHz), Varian Inova-500 (^{1}H at 499.722 MHz, ^{13}C at 125.671 MHz, ^{19}F at 470.253 MHz, ^{31}P at 202.375 MHz), Varian VNMRS-600 (^{1}H at 599.944 MHZ, ^{19}F at 564.511, ^{31}P at 242.862 MHz), or Varian VNMRS-700 (^{1}H at 699.731 MHz, ^{13}C at 175.948 MHz, ^{19}F at 658.405 MHz, ^{31}P at 283.256 MHz) spectrometer. All chemical shifts are given in ppm and coupling constants are in Hz. Longitudinal relaxation times (T_1) were measured in dilute D_2O solutions at 295 K using the inversion-recovery technique. For ^{19}F, the relaxation data were measured without proton decoupling and the chemical shifts are reported relative to fluorotrichloromethane.

^{1}H and ^{17}O Relaxometry

The proton $1/T_1$ Nuclear Magnetic Relaxation Dispersion (NMRD) profiles were measured on a fast field-cycling Stelar SmartTracer relaxometer (Mede, Pv, Italy) over a continuum of magnetic field strengths from 0.00024 to 0.25 T (corresponding to 0.01-10 MHz proton Larmor frequencies). The relaxometer operates under computer control with an absolute uncertainty in $1/T_1$ of ± 1%. The temperature was controlled with a Stelar VTC-91 airflow heater equipped with a calibrated copper–constantan thermocouple (uncertainty of ±0.1 K). Additional data points in the range 15-70 MHz were obtained on a Stelar Relaxometer equipped with a Bruker WP80 NMR electromagnet adapted to variable-field measurements (15-80 MHz proton Larmor frequency). For these ^{1}H data ca. 0.5-1.2 mM solutions of the Gd(III) complexes in non-deuterated water at neutral pH were utilized. The exact complex concentration was determined by the bulk magnetic susceptibility shift (BMS) method on a Bruker Avance III operating at 11.7 T. Other relaxation measurements were made at 1.4 T using a Bruker Minispec mQ 60 relaxometer, operating at 310K.

^{17}O NMR measurements were recorded on a Bruker Avance III spectrometer (11.7 T) equipped with a 5 mm probe and standard temperature control unit. An 8 mM

aqueous solution of the complex containing 2.0% of the ^{17}O isotope (Cambridge Isotope) was used. The observed transverse relaxation rates were calculated from the signal width at half-height.

MRI studies

Imaging studies were carried out using a 7 T Varian Unity Inova microimaging/pre-clinical system equipped with broadband capability and actively shielded gradients. For the ^{19}F MRI studies, a purpose built four turn solenoid coil (20 mm diameter, 20 mm coil length) was used for *in vitro* experiments and a ^{19}F-tuned square surface coil (30 mm, m2m Imaging Corp.) was used for *in vivo* experiments. For the ^{1}H MRI studies, *in vitro* experiments were performed with a 30 mm i.d. birdcage volume coil (Rapid Biomedical) and *in vivo* experiments were performed with a 39 mm i.d. birdcage volume coil. All coils were used for both signal excitation and reception.

For phantom studies, dilute aqueous samples (2-5 mM) were placed in Eppendorf tubes or cut down (2-3 cm) NMR tubes and positioned on the axis of the coil. For *in vivo* studies, nude mice bearing a HT29 colorectal tumour xenograft were anaesthetised with oxygen/1-2 % isofluorane (for the ^{1}H MRI studies) or with a mixture of ketamine (0.75 mg/kg) and medetomidine (0.5-1.0 mg/kg) (for the ^{19}F MRI studies). Complexes were administered intravenously as saline solutions *via* the tail vein, with doses typically 0.03 mmol/kg.

Ligand synthesis and general methods

See the ESI for additional synthesis and characterisation details.

Dialysis was performed with Dialysis Tubing Cellulose Membrane MWCO 550 D (Sigma Aldrich), Spectra/Por Dialysis Membrane MWCO 1,000 D (Spectrum Laboratories, Inc), or Float-A-Lyzer G2 filters MWCO 5,000 D (Spectrum Laboratories, Inc). All tubing was washed thoroughly with H_2O, as per manufacturer's advice. After addition of the complex to the tubing, the ends of the tubing were secured (clamps for the membranes, provided screw top for the filters) and the ensemble submerged in stirring H_2O (ca. 500 mL). The bulk H_2O was

exchanged 4 times over a 72 h period, to ensure a positive dialysis gradient was maintained. Filtering of the tubing contents and lyophilisation yielded the desired product.

Glycol chitosan was purchased from Sigma and purified by dialysis before use. After purification, the sample had a molecular weight of about 195,000 D as revealed by GPC analysis; its solubilisation in water required sonication over a period of two hours. The sample was modified to prepare a lower molecular weight polymer, by acidic digestion with 4M HCl at 50°C over 24 hours. After dialysis purification, the sample possessed an average MW of 6,590 D (*vide infra*) and exhibited higher water solubility compared to the parent system.

10-[((2-4-Ethoxycarbonyl-2-(trifluoromethyl)phenylamino)-2-oxoethyl]-1,4,7-tris(*tert*-butoxycarbonylmethyl)-1,4,7,10-tetraazacyclododecane , 1

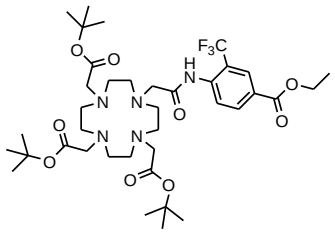

To a solution of 1,4,7-tris(*tert*-butoxycarbonylmethyl)-1,4,7,10-tetraazacyclododecane (500 mg, 0.97 mmol) and 2-chloro-N-(4-(ethoxycarbonyl)-2-trifluoromethylphenyl)-ethanamide (331 mg, 1.07 mmol) in dry CH_3CN (20 ml) under argon, was added K_2CO_3 (161 mg, 1.17 mmol) and KI (5 mg, cat.). The mixture was boiled under reflux for 24 h. After filtration, the residue was washed with CH_2Cl_2 (2 x 30 ml) and solvent removed under reduced pressure to yield a pale brown oil that was purified by column chromatography over silica gel (CH_2Cl_2 to CH_2Cl_2/10%EtOH). The resultant oil was purified by crystallization from hot diethyl ether yielding a white powder (597 mg, 78%), m.p. 185-186°C. R_f = 0.6 (silica, DCM/5%EtOH); ^{1}H NMR (500 MHz, $CDCl_3$): δ 1.26, 1.37 (27H, br, s, CH_3), 1.33 (3H, t, J = 7.0 Hz, $CH_2\underline{CH_3}$), 1.90-3.80 (24H, br, CH_2 ring and CH_2CO), 4.33 (2H, q, J = 7.0 Hz, $\underline{CH_2}CH_3$), 7.76 (1H, d, J = 8.5 Hz, aromatic H^6), 8.01 (1H, dd, J = 8.5, 1.5 Hz, aromatic H^5), 8.20 (1H, d, J = 1.5 Hz, aromatic H^3), 9.48 (1H, br, s, NH); ^{13}C

NMR (125.7 MHz, $CDCl_3$): δ 14.49 ($CH_2\underline{C}H_3$), 27.99, 28.07 (CH_3), 48.52, 52.63 (br, CH_2 ring), 55.74, 55.82, 57.01 ($\underline{C}H_2CO$), 61.64 ($\underline{C}H_2CH_3$), 82.07 ($\underline{C}$-CH_3), 123.35 (q, $^1J_{CF}$ = 274 Hz, CF_3), 124.91 (q, $^2J_{CF}$ = 32 Hz, aromatic $\underline{C}^2$-CF_3), 127.83 (aromatic C^4), 128.05 (q, $^3J_{CF}$ = 5 Hz, aromatic C^3), 128.29 (aromatic C^6), 133.23 (aromatic C^5), 139.60 (aromatic C^1), 165.26 (COOEt), 172.53, 172.63, 172.75 (C=O); ^{19}F NMR (188 MHz, $CDCl_3$): δ -60.51 (CF_3); ESI/MS$^+$ m/z 810.4 $[M + Na]^+$; MS Calcd for $C_{38}H_{60}N_5O_9F_3Na$ 810.4235. Found 810.4224.

The structure of the sodium complex of **1** was confirmed by single crystal X-ray diffraction study of the NaBr adduct, CCDC 945380. The crystal grown from diethyl ether was mounted in inert oil and transferred to the cold gas stream of the diffractometer.

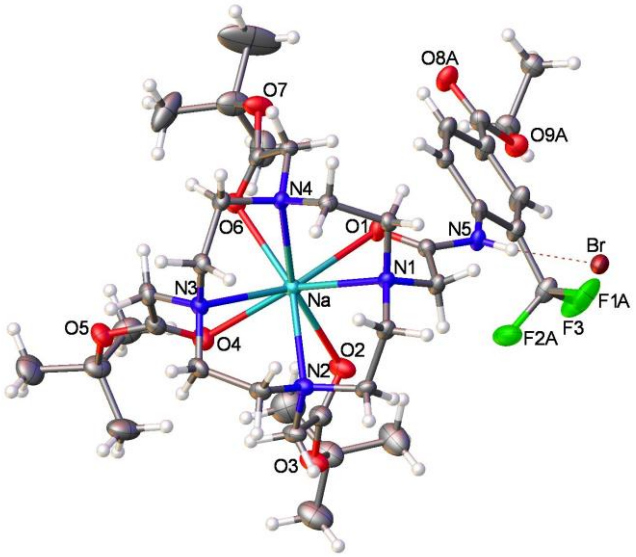

Figure 1 View of the sodium complex of the triester intermediate, **1**, showing the position of the CF_3 group with respect to the bound metal ion.

Crystal data: $[C_{38}H_{60}N_5O_9F_3Na]^+Br^-\cdot$½ Et_2O, M =927.87, a = 27.177(1) Å, c = 12.4222(4) Å, V = 9175.0(6) Å^3, T = 120(2), tetragonal space group P4/n (no. 85), Z = 8, μ(Mo-$K\alpha$) = 0.975, 119016 reflections measured, 13394 unique (R_{int} = 0.088), final R_1= 0.037 [$I \geq 2\sigma(I)$], wR_2 = 0.101 (all data). The CF_3 group is disordered, by libration about the C(arene) and one of the fluorine atoms, between two alternative orientations with occupancies of 0.8 and 0.2, (Figure 1). The shortest intramolecular F…Na distances for these sites are 6.054(2) and 6.14(2) Å. Given that the ionic radius for sodium in 8–coordination is 1.32 Å (*vs* 1.21 Å for Ho^{3+}), the slightly shorter distances here are in line with the measurements estimated by NMR analysis of the variation of

the 19-F relaxation rate with field, that gave the separation of the CF_3 group from the lanthanide ion as 6.3 (±0.2)Å. [4c]

Preparation of partially hydrolysed glycol chitosan (MW~6,590)

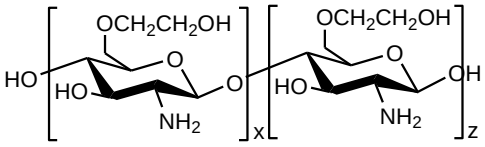

Glycol chitosan (1 g, Sigma) was dissolved in a solution of hydrochloric acid (75 ml, 4M) and any insoluble material was manually removed from the solution. The solution was left stirring at 50˚C for 24 h, and then dialysed (cut off 12,000D) against Purite water until the pH of the tube contents reached neutrality (2 days). Lyophilisation yielded a light off-white powder (560 mg). Anal Found C, 37.84; H, 6.92; N, 5.57%. For GPC analysis, see Table 1.

[Ho.L^1(H_2O)-chitosan] conjugate

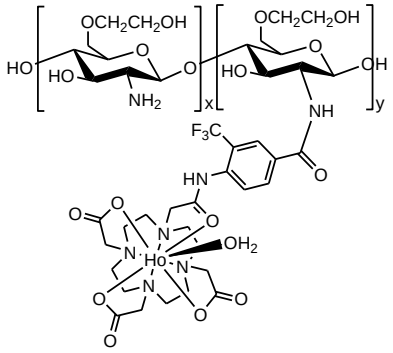

To a stirred suspension of **[Ho.L^1(H_2O)]** (260 mg, 345 mmol) in dry DMF (2.2 ml) under argon was added N-methylmorpholine (57 ml, 518.0 mmol) and finally TBTU (166 mg, 518.0 mmol). The solution was stirred for 30 min at room temperature, and an aqueous solution of glycol chitosan (MW~6,590) (40 mg in 0.4 ml of water) was added dropwise. The mixture was left stirring overnight at 40˚C. The crude was diluted with water and dialysed against Purite water over 2 days (cut off 1,000D). The solution was lyophilised to yield a light brown solid. ^{19}F NMR (376.3 MHz, D_2O): δ-

56.8 (CF_3, $\omega_{1/2}$ = 257 Hz); Anal: Found C, 37.65; H, 4.93; N, 7.53, Ho = 13.0 %. For GPC analysis, see Table 1.

Glycol chitosan Gd complex conjugate

Prepared as described for the holmium analogue; Anal Found C, 34.84; H, 4.64; N, 6.98, Gd = 12.9%. r_{1p} = 14.9 $mM^{-1}s^{-1}$ (310K, 20MHz). For GPC analysis: Table 1.

Glycol chitosan Dy complex conjugate, [Dy.L^3-chitosan]

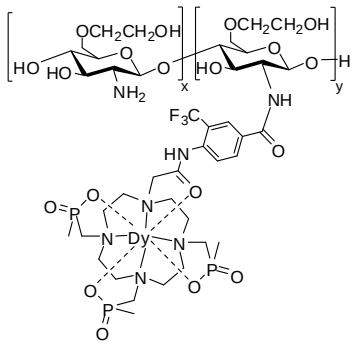

The complex **[Dy.L^3]** (157 mg, 0.184 mmol) was dissolved in anhydrous DMF (2 mL) to which NMM (30 μL, 0.276 mmol) and TBTU (89 mg, 0.276 mmol) were added. The mixture was stirred at rt for 30 min under argon, before glycol chitosan (20 mg, MW ≈ 6500 D) dissolved in H_2O (0.2 mL) was added. The mixture was left stirring at 40°C for a further 18 h, before the solution was diluted with H_2O (10 mL) and dialysed against Purite water for 48 h (1000 MW cut-off), with the bulk solvent water refreshed periodically. The solvent was removed under reduced pressure, before the residue dissolved in H_2O and dialysed for a second time (5000 MW cut-off). The solution was lyophilised to yield a white solid (48 mg). ^{19}F NMR (376 MHz, D_2O, pD 6.5): δ = -65.7; Mean M_w = 14,600 D by GPC analysis, (Table 1). Found: Dy = 10.6 %.

The analogous [**Gd.L^3-chitosan**] conjugate was made by a parallel method. Found: Gd = 9.7%. r_{1p} = 12.4 $mM^{-1}s^{-1}$ (310K, 60 MHz). The relaxivity of the complex did not change over the pH range 6 to 7.4, but at higher pH values it increased, reaching a

value of 27.2 $mM^{-1}s^{-1}$ (pH 11). An apparent pK_a of 9.5 (±0.2) can be tentatively associated with the changes in hydration associated with amide deprotonation and the deprotonation of residual NH_3 protons on the chitosan.

Table 1 Gel permeation chromatography (GPC) data for partially hydrolysed glycol chitosan precursor and its conjugates

Sample	M_w [a]	M_n [b]	PDI [c]
Glycol-chitosan	6,590	2,250	2.9
[Ho.L^1] conjugate	16,200	4,500	3.6
[Gd.L^1] conjugate	15,950	4,155	3.8
[Gd.L^3] conjugate	13,800	6,890	2.0
[Dy.L^3] conjugate	14,600	7,620	1.9

Mean values obtained from two successive runs. [a] calculated molecular weight averages expressed as the pullulan polysaccaride equivalent molecular weights; [b] number average molecular weights; [c] polydispersity (M_w/M_n).

Results and Discussion

Complex and conjugate synthesis

The syntheses of the ligands $\mathbf{L^1}$ and $\mathbf{L^3}$ have been detailed recently [5a,5b]. The lanthanide(III) complexes derived therefrom were purified by preparative scale reverse-phase HPLC. High resolution accurate mass spectrometry confirmed the constitution of the complex, with experimental isotope patterns showing good correlation to those calculated. The ^{19}F NMR spectrum (D_2O, 295K 9.4T) revealed the presence of one major (87%) and six minor species in solution, consistent with the

formation of one predominant stereoisomer, amongst the 32 NMR distinguishable isomers that are theoretically possible in this system [10].

A representative synthesis of the conjugate, [**Dy.L^3-chitosan**] is outlined in Scheme 2. The carboxylic acid group of [**Dy.L^3**] was converted to an active ester, by reacting with *o*-(benzotriazol-1-yl)-*N,N,N′,N′*-tetramethyluronium tetrafluoroborate (TBTU) and 4-methylmorpholine (NMM) in DMF. After stirring for 1 h, to allow formation of the active ester, a concentrated aqueous solution of partially hydrolysed glycol chitosan (average MW 6,590 D) was added and the mixture stirred for a further 36 h. Purification of the conjugate was achieved by extensive dialysis to remove unreacted coupling reagents and excess complex.

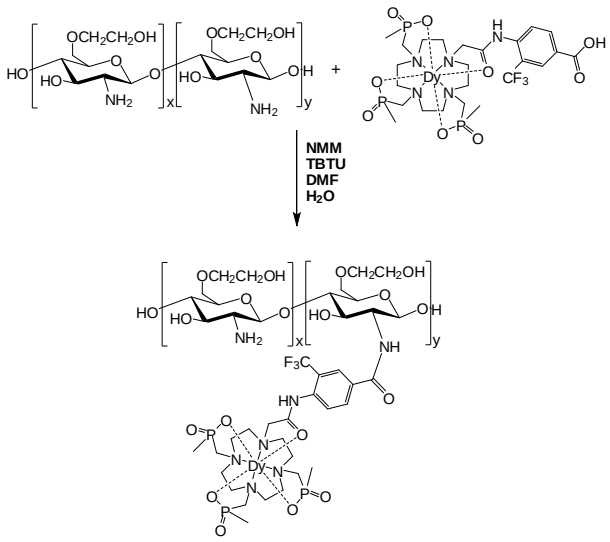

Scheme 2 Synthesis of the chitosan conjugate complex, [**Dy.L^3-chitosan**].

To determine the average size and mean number of complexes conjugated to chitosan, the complex was analyzed by aqueous gel permeation chromatography (GPC, Table 1 above). By comparing the molecular weights of the unreacted complex and glycol chitosan with that of [**Dy.L^3-chitosan**], it was calculated that there are around 8.5 complexes bound to each molecule of glycol chitosan. As glycol chitosan is a polydisperse material, such values are averages for the whole system. Low solubility in water had been observed in preliminary work with chitosan-conjugates derived from a higher MW precursor, but no solubility issues were seen with the conjugate reported here, at the concentrations employed (up to 10 mM).

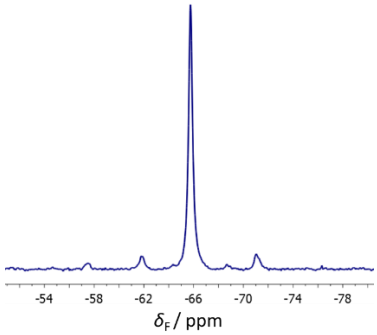

Figure 2 ^{19}F NMR spectrum of [**Dy.L^3-chitosan**] (D_2O, 9.4 T, pD 7.4, 0.1 M NaCl, 298 K), showing the presence of one major (86%) and six minor isomeric species in solution.

The ^{19}F NMR spectrum of [**Dy.L^3-chitosan**] displayed one principal resonance (86 %), indicating equivalence of each complex in the conjugated adduct (Fig. 2). The occurrence of one major resonance is required for *in vivo* applications to ensure that signal intensity is maximised. Relaxation rates were measured at 4.7 and 9.4 T, (Table 2), along with the data for the parent complex, [**Dy.L^3**], and [**Ho.L^1(H$_2$O)chitosan**].

Table 2 ^{19}F NMR longitudinal and transverse relaxation rates at two magnetic fields (4.7 and 9.4 T, 295K, D_2O) for Dy and Ho complexes.

Complex	δ_F / ppm	4.7 T		9.4 T	
		R_1 / Hz	R_2 / Hz	R_1 / Hz	R_2 / Hz [(a)]
[Dy.L^3]	-64.5	110	217	186	440
[Dy.L^3-chitosan]	-65.7	108	176	183	367
[Ho.L^1)-chitosan]	-56.8	56	741	100	807
[Ho.L^2(H$_2$O)]	-56.8	59	173	123	292

(a) R_2 values were estimated as ($\pi\omega_{1/2}$) for a Lorentzian line fit.

There is a substantial improvement in relaxation rates for the phosphinate conjugate, [**Dy.L^3-chitosan**], over the carboxylate based system, [**Ho.L^1-chitosan**]. Such a difference is most likely due to a longer electronic relaxation time T_{1e}, in the former series, associated with a bigger static and transient ligand field [11]. The longitudinal relaxation rate, R_1, is almost twice as large for the dysprosium system, coupled with a sizeable reduction in the transverse relaxation rate, R_2, calculated from the linewidth.

Each of these factors will serve to improve signal intensity and the combination of the improvement in both relaxation rates suggested considerable scope for acquisition of a ^{19}F MR image with [**Dy.L^3-chitosan**].

Proton relaxation studies with the Gd complex conjugate of [**Gd.L^1(H$_2$O)**]

The relaxivities of a diluted solution of the Gd-chitosan conjugate in water and of the monomeric Gd complexes, [**GdL^1(H$_2$O)**], were measured at 60 MHz and 37°C. The parent complex had a value of 4.62 $mM^{-1}s^{-1}$, which is typical of such a mono-aqua [**Gd.DO3A-monoamide**] complex. [15] In the glycol chitosan conjugate, [**Gd.L^1-chitosan**], the relaxivity was 11.2 $mM^{-1}s^{-1}$. Such an enhancement is associated with slower rotation of the Gd complex, increasing the value of the rotational correlation time τ_R, leading to a higher relaxivity. [15] In theory, the increased viscosity of the solution, due to the presence of the dissolved polymer, may also be responsible for an increased relaxivity as molecular tumbling is slowed down. To confirm whether the higher relaxivity value of the conjugate was related to a change in solution viscosity or to the presence of the covalently linked macromolecule, a control experiment was performed. A solution containing the Gd complex and the precursor 6600 MW glycol chitosan was prepared and its relaxivity measured at 60 MHz at 37°C. The value obtained was 4.79 $mM^{-1}s^{-1}$, which is very similar to that of the parent complex. Such behaviour shows that the observed increased relaxivity is caused by the presence in solution of the covalently bonded conjugate.

The Gd conjugate can be employed as a conventional contrast agent in proton MRI by virtue of its ability to enhance the rate of relaxation of the bulk water protons. The relaxation behaviour was assessed and compared to the behaviour of the parent Gd complex. Variable temperature ^{17}O NMR measurements for [**Gd.L^1(H$_2$O)**] were performed in ^{17}O-enriched water (Fig. 3) and the data analyzed using the standard Swift-Connick methodology [16] to obtain an estimate of the water exchange lifetime τ_M. The analysis gave a τ_M value of 0.92 μs at 298 K, similar to related mono-amide derivatives based on [Gd-DO3A] [15]

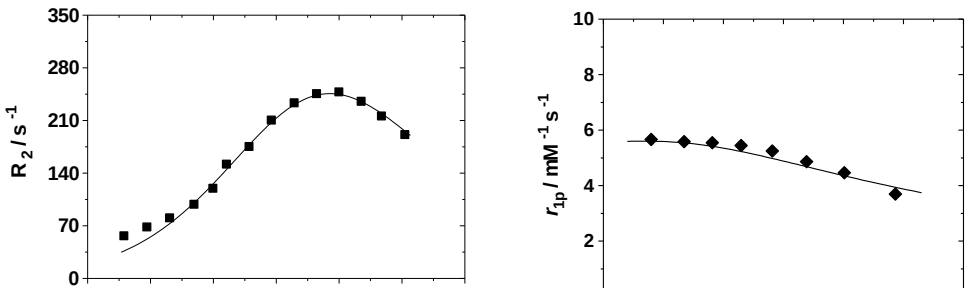

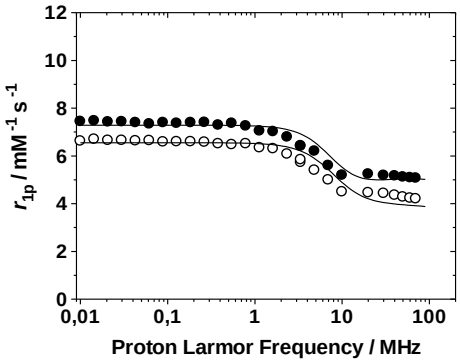

Figure 3 Proton relaxivity study for [**Gd.L^1(H$_2$O)**] showing the fit (*line*) to the measured data: (*top left*) ^{17}O R_2 vs temperature profile measured at 11.7 T (500 MHz); (*top right*) relaxivity vs temperature profile measured at 20 MHz and pH 7.2; (*bottom*) $1/T_1$ NMRD profiles at 298K (*filled circles*) and 310K (*open circles*).

The relaxivity profiles as a function of temperature and magnetic field allowed information to be deduced on the water exchange rate and various associated parameters used in the Solomon-Bloembergen-Morgan equations. Fitting was undertaken assuming the presence of one coordinated water molecule (q = 1), at a distance of 3.0 Å from the metal ion (r_{GdH}) and fixing the values for the distance of closest approach to the paramagnetic centre of the outer sphere solvent molecules (a = 4.0 Å) and for their diffusion coefficient (D = 2.24 and 3.10 cm^2 s^{-1}, at 298 and 310K respectively). The values of the main parameters that describe the proton relaxation behaviour of the complex are reported (Table 3) and are consistent with those expected for such low molecular weight mono-aqua complexes, with an additional contribution modelled as two more distant (q'') water molecules, located on average 4.4 Å from Gd. It is worth noting that this analysis is not entirely rigorous and provides only an estimate of the magnitude of the contribution of second sphere

solvent molecules to the overall relaxivity of the complexes. Clearly, a number of water molecules at different distances from the metal ion and with different lifetimes all contribute together to the observed relaxivity. The contribution of this mechanism is equivalent to that of two water molecules at a distance of 4.4 Å from Gd or to that of a single molecule localized at about 3.9 Å [15]

Table 3 Relaxation data for [**GdL^1(H$_2$O)**]

Parameter [a]	**298 K**
r_{1p} (mM^{-1} s^{-1})	5.2
τ_M (μs)	0.92
τ_R (ps)	83
τ_V (ps)	16
Δ^2 ($s^{-2} \times 10^{19}$)	8.8
q''	2
r'' (Å)	4.4

[a] r_{1p} is the proton relaxivity; τ_M is the water exchange lifetime; τ_R is the rotational correlation time; τ_V is the correlation time for the ZFS modulation; Δ^2 is the mean-square zero field splitting energy; q is the number of inner sphere water molecules; q'' is the number of second sphere water molecules and r'' their distance from Gd.

For the Gd-conjugate, the relaxivity behaviour as a function of temperature and magnetic field were also measured (Fig. 4). In the case of macromolecular conjugates, the analysis of NMRD profiles requires a different approach, since the presence of a relatively fast local rotation of the complex, compared to the slow motion of the macromolecule, needs to be considered. This is possible by incorporating the description of the rotational dynamics according to the 'model-free' Lipari–Szabo approach into the Solomon-Bloembergen-Morgan equations for the inner sphere relaxation mechanism. [17,18] This model allows the contribution of the global rotation of the whole paramagnetic system (τ_{RG}) to be separated from the contribution

of a faster local motion (τ_{RL}) associated with free rotation of the complex via the pendant arm.

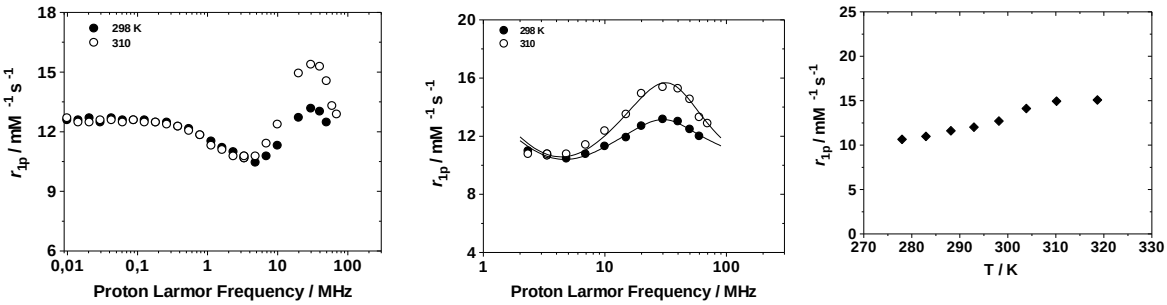

Figure 4 Proton relaxivity studies for [**Gd.L^1(H$_2$O)-chitosan**]: (*right*) relaxivity *vs* temperature profile measured at 20 MHz; (*left*) $1/T_1$ NMRD profiles at 298K (filled circles) and 310 K (open circles); (*centre*): higher frequency NMRD profiles analyzed with the Lipari-Szabo model [17,18]

The correlation of the two types of motions is described by the parameter S^2 whose value ranges between zero (completely independent motion) and one (totally correlated motion). The fitting of the NMRD profiles with the Lipari-Szabo model is also shown (Fig. 4 centre) and the resulting best-fit parameters reported in Table 4.
For the macromolecular conjugates, only the high field region was analyzed because of the inadequacy of the SBM model to reproduce the low fields data when the tumbling motion is so long. The parameters Δ^2 and τ_V were treated simply as fitting parameters and do not have a precise physical meaning. The values of q, r_{GdH}, and τ_M were assumed to be identical to those found for the parent Gd complex.

The results are consistent with the presence of a slow tumbling motion of the system, superimposed on fast local rotation of the Gd-chelates. [19] This is underlined by the low value of S^2. Moreover, the relaxivity reaches a maximum value at 30 MHz (typically found at 20 MHz for more 'rigid' systems) of 15.9 mM^{-1}s^{-1} at 310 K. This is probably a consequence of a relatively fast internal motion (0.49 ns) rather than the slow global rotation (6 ns). The relatively long residence lifetime of the inner sphere water molecule limits the relaxivity of the slowly tumbling system. Indeed, the relaxivity increases significantly with temperature. A maximum value is reached

around 315 K. A simple simulation revealed that the relaxivity would increase to 27 if τ_M was 20 ns at 298 K and 20 MHz.

Table 4 Relaxation data for [**Gd.L^1(H$_2$O)-chitosan**].[a]

parameter	298 K	310 K
r_{1p} (mM^{-1} s^{-1})[b]	12.7	14.9
τ_M (μs)	0.92	0.63
τ_{RL} (ns)	0.58	0.49
τ_{RG} (ns)	8	6
S^2	0.09	0.17
τ_V (ps)	21	20
Δ^2 (s^{-2} × 10^{19})	1.4	1.4
q	1	1
a (Å)	4.0	4.0
D (cm^2 s^{-1} × 10^{-5})	2.24	3.10

[a] τ_{RG} is the global rotation of the whole paramagnetic system; τ_{RL} the local motion contribution; S^2 the correlation between the global and local motion; a the Gd-H distance for the outer sphere water molecules and D the relative diffusion coefficient; [b] at 20 MHz

Proton MRI studies with [Gd.L^1(H$_2$O)-chitosan]

MRI studies with the [Gd.L^1(H$_2$O)-chitosan] conjugate were performed using nude mice bearing an HT29 colorectal tumour xenograft as animal model, with the aim of assessing the distribution and the tumour uptake of the conjugate. The mice were anaesthetised with a mixture of oxygen/1-2% isoflurane, placed in the MR system and scout images obtained. A Dynamic Contrast Enhanced (DCE) MRI study was performed in a single 2 mm slice containing the tumour and acquiring a total of 100 over a 10 min acquisition period. Five baseline ^{1}H MR images were collected (30 s) after which 200 μl of a 2.5 mM solution of the Gd complex-chitosan conjugate was administered by manual intravenous injection in the tail during the sixth image. Each mouse (~30 g, n=4) received a dose of 0.017 mmol/kg. An almost immediate contrast

enhancement (<1 min) was observed after administration of the conjugate, both in the tumour and the bladder (Fig. 5). The compound was well tolerated by the animals.

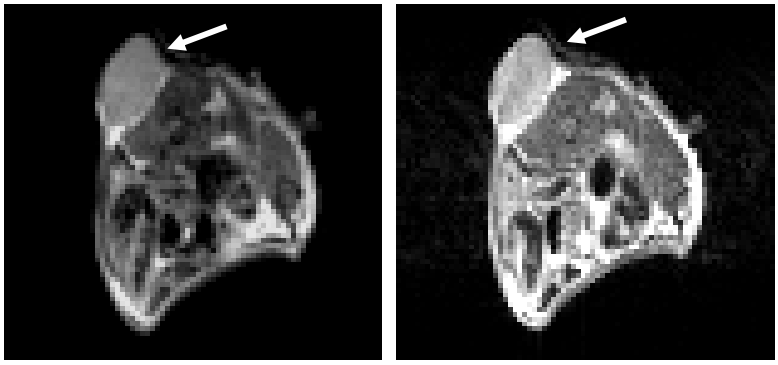

Figure 5 T-1 weighted ^{1}H MR images : *left* before and *right* after administration of [**Gd.L^{1}(H$_2$O)-chitosan**] (0.017 mmol/kg dose) in a nude mouse bearing an HT-29 colorectal tumour xenograft (arrow).

The tumour area was analyzed to measure the mean signal intensity profile as a function of time (Fig. 6). Rapid and selective uptake of the conjugate was observed in the tumour, within the 10 min acquisition time. This behaviour is most probably related to an EPR effect (enhanced permeability and retention) that is characteristic of such medium molecular weight conjugates. [15] This leads to their selective accumulation in tumours through the increased fenestration of the blood vessels in the area and subsequent slower rates of clearance from the site. This represents a potential advantage of such conjugates compared to lower molecular weight Gd complexes, which in healthy animals are usually more rapidly excreted via the kidney or liver and accumulate in the bladder more quickly after administration.

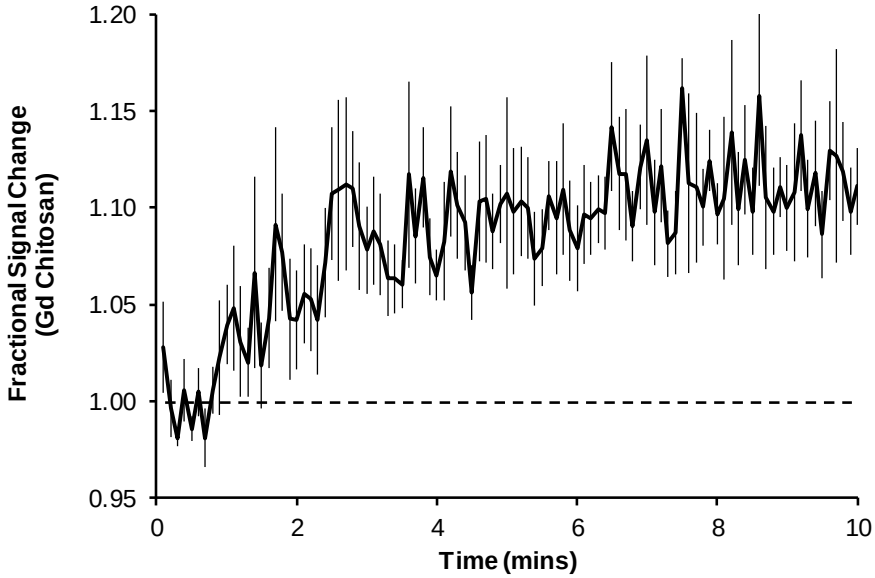

Figure 6 Temporal profile of the mean intensity of the tumour area, showing the increase in signal intensity following intravenous administration of [**Gd.L^1(H$_2$O)-chitosan**] (17 μmol/kg); the data shown represents the mean intensity value averaged over four animals (±SEM). Fluctuations in the mean signal reflect effects of uncompensated respiratory motion; however, the overall long term signal trend is clear.

The presence of conjugate in the bladder and liver is consistent with both renal and biliary excretion, indicating that the conjugate is being eliminated from the body by each of the major pathways. The increase of the mean signal intensity reached the value of 1.22. Corresponding values obtained using the commercially available Gd contrast agent Prohance and in analogous experiments were in the range 1.20-1.28, although the latter was administered at a higher dose, *i.e.* 0.1 mmol/kg against 0.017 mmol/kg for the Gd-chitosan conjugate.

A similar scouting experiment was undertaken with [**Gd.L^3-chitosan**] to track its uptake, this time examining mice (4) bearing a related HCT-116 colorectal tumour xenograft. Conventional dynamic gradient spin-echo MR scans (6.66 s temporal resolution) were taken pre (6 scans) and post-injection, over a 13 minute period following a single tail-vein injection of an 0.03mmol/kg dose of the conjugate. The data was analysed in terms of the change in intensity (pre *vs* post contrast (13 min.) in the tumour, kidney, liver, bladder and muscle (Fig. 7). The changes in intensity for

tumour to liver and tumour to muscle at this time point were 2:1 and 5:1 respectively, with again clear evidence for predominant renal clearance, with similar retention over this time interval in the tumour and liver tissues.

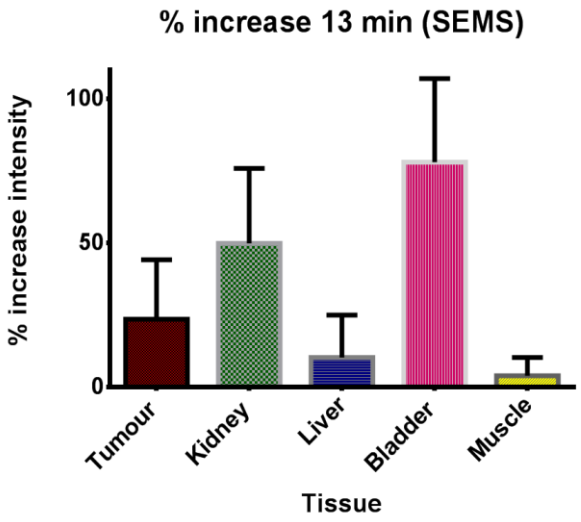

Figure 7 Change in signal intensity in proton MR images taken 13 minutes after tail vein injection of an 0.03mmol/kg dose of [**Gd.L^3-chitosan**]

^{19}F MR Imaging studies

A ^{19}F MRI dynamic experiment was performed using the [**Ho.L^1(H$_2$O) chitosan**] conjugate, using a dose of 0.034 mmol/kg on the HT-29 animal model. A similar dynamic sequence was used to acquire ^{19}F MR images over one hour. No fluorine signal was detected after administration of the conjugate, most likely due to the rather broad linewidth observed (750 Hz) that led to T_2 losses in signal acquisition and hence insufficient signal intensity for observation on the experimental timescale.

Preliminary imaging studies with [**Dy.L^3-chitosan**] were carried out using a 3D gradient echo sequence (Fig. 8) with a four turn solenoid coil (20 mm diameter, 20 mm coil length). The R_1 and R_2 values were estimated to be 145 and 270 Hz, respectively, leading to a calculated Ernst angle of 60.7^o for a repetition rate, T_R, of 25 ms. With a total scan duration of 131 s, good quality images were acquired at a resolution of 1x1x1 mm^3. Shorter echo times, T_E (2.07 ms), were applied in order to

minimise R_2 loss. The resulting mean signal-to-noise ratio (SNR) from the 1x1x1 mm^3 volume element was calculated to be 9.1, which was a significant improvement on previously studied compounds when scaled for comparison (to take account of differences in total examination time and concentration). These results were promising for further investigation, and *in vivo* experiments were undertaken.

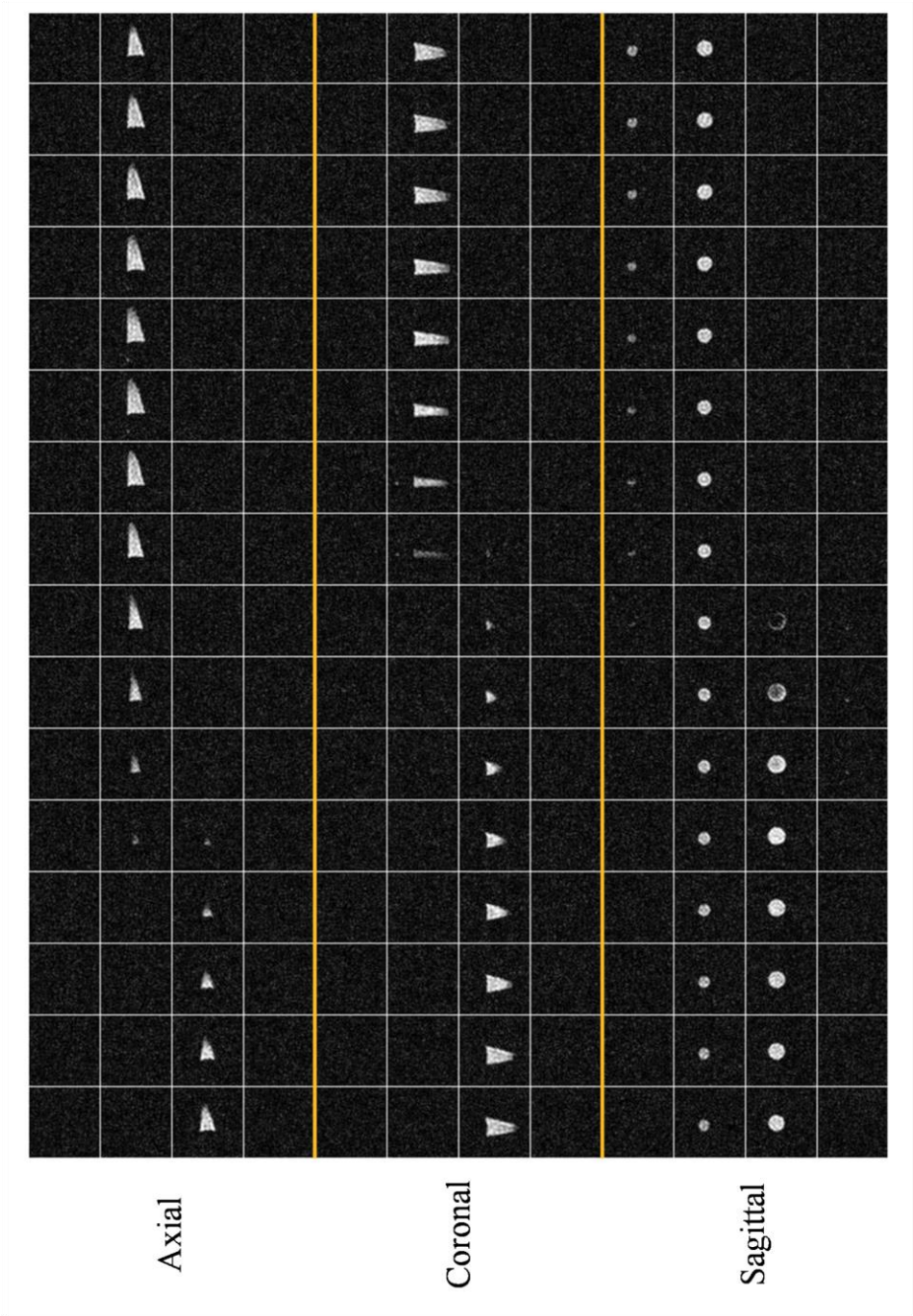

Figure 8 ^{19}F MR phantom images of [**Dy.L^3-chitosan**] contained in an Eppendorf tube (2 mM complex, H_2O, 0.1 M NaCl, 7 T, 295 K, 3D gradient echo sequence, 1x1x1 mm^3 resolution, T_R = 4.91 ms, T_E = 2.07 ms, flip angle = 60.7^o, 26 averages, scan duration = 131 s, mean SNR from 1x1x1 mm^3 = 9.1).

Preliminary *in vivo* studies were carried out on SCID male mice (30 g) with HT29 tumours. Measurements were taken 10-14 days after inoculation when tumours were around 10 mm in diameter, with the mouse anaesthetised with a mixture of ketamine (0.75 mg/kg) and medetomidine (0.5-1.0 mg/kg).). The animal was positioned on a ^{19}F tuned square surface coil (30 mm coil length) and the MR system was calibrated using a reference vial placed between the animal and the coil which was subsequently removed remotely without disturbing the animal. A solution (5 mM) of [**Dy.L^3-chitosan**] was then administered by intravenous injection in the tail. The mouse received 250 µL of the solution, corresponding to a dose of 0.037 mmol/kg. Immediately following injection simple detection of the [Dy.L^3-chitosan] was confirmed using unlocalised spectroscopy which demonstrated both the expected resonance and a second unidentified resonance shifted by -4900Hz (-17ppm), which was not seen from the reference sample (Fig.9). The nature of this second species remains uncertain, at present. While the *in vitro* data (Fig. 8) could be collected using a standard imaging sequence, the linewidths *in vivo* were broader and localised spectral detection was therefore employed using a 2D spectroscopic imaging approach allowing much shorter T_E and hence reduced R_2 related signal loss. The distribution of the complex within the animal was clearly mapped.

Figure 9 *In vivo* data showing detection of ^{19}F signal from [**Dy.L^3-chitosan**]. Left: stack plot of unlocalised post-injection ^{19}F spectra (35µs hard excitation pulse, flip angle = 90^o,

sweep width = 40 kHz, T_R = 55ms, 2048 averages, scan duration = 113s). Also shown is the signal from a reference vial placed on the coil for pulse calibration. Right: representative conventional gradient echo T_1 weighted MRI and spectroscopic imaging data with effective in-plane voxel size of ~3mm (35ms hard excitation pulse, flip angle = 90°, sweep width = 40 kHz, T_R = 55ms, T_E = 0.22 ms, 48 averages, scan duration = 169s, in-plane resolution 4x4mm, zero-filled to 2x2mm). Variation in the spatial distribution of the resonances at 0 and -4900 Hz are clearly seen in the spectroscopic imaging data. Gridlines on the image indicate the equivalent location of each spectrum in the MRSI dataset.

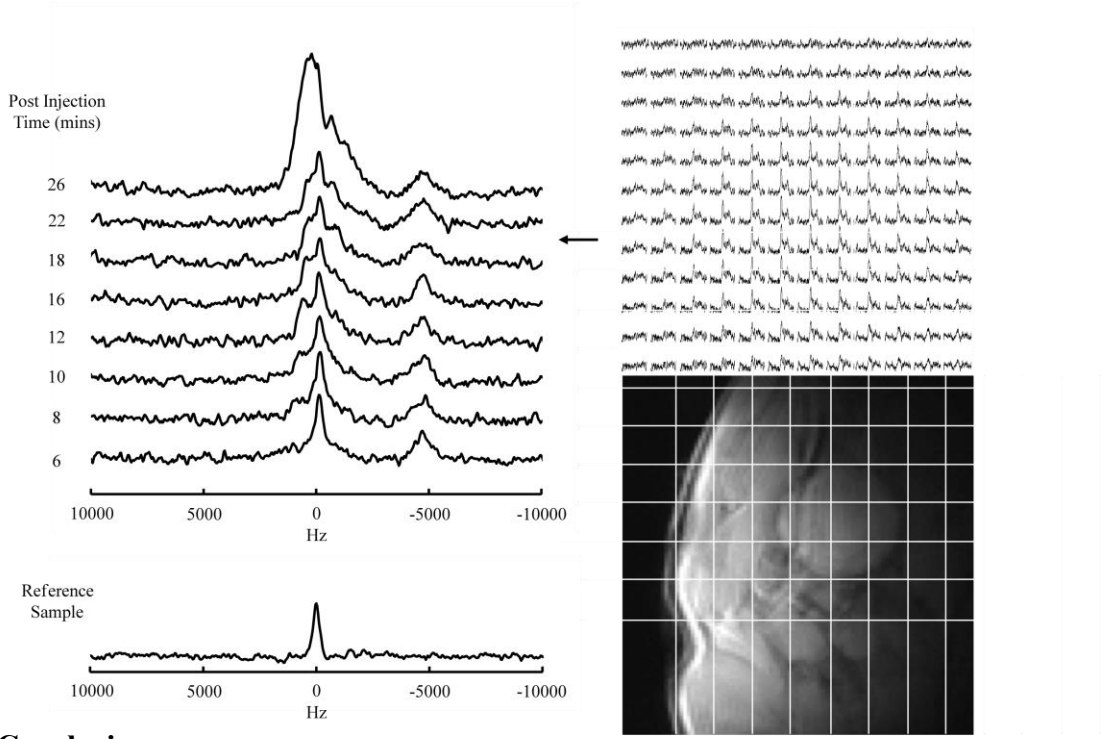

Conclusions

This proof-of principle study introduces the idea of a fast-relaxing fluorinated probe in a conjugate that clears relatively slowly from the body. These features allow 19-F chemical spectral imaging studies to be undertaken at doses that are in the range of those used in the clinically approved series of gadolinium contrast agents. There remains a need to understand better the origins of the line-broadening phenomenon observed in vivo, as this limits the resolution and sensitivity of the method, with the materials examined herein. A tentative suggestion may be that there is some non-covalent association in vivo with endogenous macromolecules, e.g. protein that gives rise to some chemical exchange broadening.

The work has wider implications, as it demonstrates that a fast-relaxing spin label can be observed *in vivo* on timescales that are amenable to modern imaging methods. Such behaviour holds, provided that the label can be observed selectively in the appropriate spectral window. In the systems described here, the extension to Gd-enhanced imaging studies of the water signal is particularly useful, as it allows genuine dual imaging protocols to be developed, observing water and probe signals sequentially, simply be permuting the lanthanide ion in the same ligand or conjugate structure.

The extension of these ideas to the use of paramagnetically shifted proton spin labels ('PARASHIFT' proton MR) is being reported concurrently [20] for related macrocyclic structures, labelled with a *t*-butyl reporter resonance that is around 6 to 7 Å from the paramagnetic centre.

Acknowledgements

We thank EPSRC and CR-UK for support, Dr Andrei Batsanov for determination of the X-ray crystal structure and Dr Alan Kenwright for certain NMR relaxation experiments in vitro.

References

1. (a) Zhu X.-H, Zhang N, Zhang Y, Ugurbil K, Chen W (2005) NMR Biomed 18: 83; (b) Yu J.-X, Hallac RR, Chiguru S, Mason RP (2013) Progr Nucl Magn Reson Spectrosc 70: 25-49; (c) Kitamura M, Suzuki T, Abe R, Ueno T, Aoki S, (2011) Inorg Chem 50: 11568–11580.
2. Ruiz-Cabello J, Barnett BP, Bottomley PA, Bulte JWM, (2011) NMR Biomed 24: 114.
3. (a) Flögel U, Ding Z, Hardung H, Jander S, Reichmann G, Jacoby C, Schubert R, Schrader J (2008), Circulation 1118: 40; (b)
4. (a) Kenwright AM, Kuprov I, De Luca E, Parker D, Pandya SU, Senanayake PK, Smith DG(2008) Chem Commun 2514-2515; (b) Senanayake PK, Kenwright AM, Parker D, van der Hoorn, SK (2007), Chem Commun 2923-2294; (c) Chalmers KH, De Luca, E, Hogg NHM, Kenwright AM, Kuprov I, Parker D, Botta M, Wilson JI, Blamire AM (2010) Chem Eur J 16:134-148.

5. (a) Chalmers KH, Botta M, Parker, D (2011) Dalton Trans 40: 904-913; (b) Harvey P, Chalmers KH, De Luca E, Mishra A, Parker D, (2012) Chem Eur J, 18: 8748-8757; (c) Harvey P, Kuprov I, Parker D (2012) Eur J Inorg Chem, 2015-2022.
6. Yu J.-X, Kodibagkar VD, Liu L, Zhang Z, Liu L, Magnusson J, Liu Y (2013) Chem SCi 4: 2132-2137.
7. (a) Schmid F, Holtke C, Parker D, Faber C, (2013) Magn Reson Med 69: 1056-1062; (b) Chalmers KH, Kenwright AM, Parker D, Blamire AM (2011) Magn Reson Med , 66: 931-936.
8. (a) Harrison A, Walker CA, Pereira KA, Parker D, Royle L, Pulukoddy PK, Norman TJ (1993) Magn Reson Imaging 11: 761-770; (b) Pulukoddy PK, Norman TJ, Parker D, Royle L, Broan CJ (1993) J Chem Soc Perkin Trans 2 605-620.
9. Harrison A, Walker C, Cox JPL, Jankowski KJ, Parker D, Sansom J, Eaton MAW, Beeley NRA, Millican AT (1991) Nucl Med Biol 18: 469-476.
10. Aime S, Botta M, Parker D, Williams (1995) Dalton Trans 2259-2266.
11. Funk AM, Fries PH, Harvey P, Kenwright AM, Parker D (2013) J Phys Chem A 117: 905-917.
12. Nam T, Park S, Lee SY, Park K, Choi K, Song IC, Han MH, Leary JJ, Yuk SA, Kwon IC, Kim K, Jeong SY. (2010) Bioconjug Chem 21: 578-582.
13. Son JY, Jang JS, Cho YW, Chung H, Park R-W, Kwon IC, Kim I-S, Park JY, Seo SB, Park CR, Jeong SY (2003) J Controlled Rel 91: 135-145.
14. Lee SJ, Koo H, Lee D-E, Min S, Lee S, Chen X, Choi Y, Leary JF, Park K, Jeong SY, Kwon IC, Kim K, Choi K (2011) Biomaterials 32: 4021-4029.
15. Caravan, P, Ellison JJ, McMurry TJ, Lauffer RB (1999) Chem Rev 99: 2293.
16. Swift TJ, Connick RE (1962) J Chem Phys 37: 707.
17. Lipari G, Szabo A (1982) J Am Chem Soc 104: 4546.
18. Lipari G, Szabo A (1982) J Am Chem Soc 104: 4559.
19. (a) Zhang Z, Greenfield M T, Spiller M, McMurry T J, Lauffer R B, Caravan P (2005) Angew Chem Int Ed 44: 6766 –6769; (b) Botta M, Tei L (2012) Eur J Inorg Chem 1945–1960.
20. Harvey P, Blamire AM, Wilson JI, Finney K-LNA, Funk AM, Senanayake, PK, Parker D, (2013) *Chem Sci*, accepted.